Mon. Not. R. Astron. Soc. **335,** 177–188 (2002)

Correlated multiwavelength emission from the X-ray-bright Seyfert galaxy III Zw 2

N. J. Salvi,[1⋆] M. J. Page,[1] J. A. Stevens,[1,2] K. Wu,[1] K. O. Mason,[1] M. F. Aller,[3] H. D. Aller,[3] H. Teräsranta,[4] E. Romero-Colmenero,[5] F. A. Cordova[6] and W. C. Priedhorsky[7]

[1]*Mullard Space Science Laboratory, University College London, Holmbury St Mary, Dorking, Surrey RH5 6NT*
[2]*Astronomy Technology Centre, Royal Observatory, Blackford Hill, Edinburgh EH9 3HJ*
[3]*Astronomy Department, University of Michigan, Ann Arbour, MI 48109-1090, USA*
[4]*Metsähovi Radio Observatory, Metsähovintie, FIN-02540 Kylmälä, Finland*
[5]*South African Astronomical Observatory, PO Box 9, Observatory 7935, South Africa*
[6]*Department of Physics, University of California, Santa Barbara, CA 93106, USA*
[7]*NIS Division, Los Alamos National Laboratory, Los Alamos, NM 87545, USA*

Accepted 2002 April 23. Received 2002 April 19; in original form 2002 January 28

ABSTRACT

The X-ray-bright Seyfert 1 galaxy III Zw 2 was observed with *XMM–Newton* in 2000 July. Its X-ray spectrum can be described by a power law of photon index $\Gamma = 1.7$ and an extremely broad (FWHM $\sim$ 140 000 km s^{-1}) Fe Kα line at 6.44 keV. The iron line has an equivalent width of $\sim$800 eV. To study the long-term X-ray behaviour of the source we have analysed 25 yr of data, from 1975 to 2000. There is no evidence of significant intrinsic absorption within the source or of a soft X-ray excess in the *XMM* or archival data. We do not detect rapid X-ray variability (a few $\times 10^3$ s) during any of the individual observations; however, on longer timescales (a few years) the X-ray light curve shows 10-fold flux variations. We infer a black hole mass of $\sim 10^9$ M$_\odot$ (from Hβ FWHM) for III Zw 2 which is much higher than some previous estimates.

A comparison of X-ray variability with light curves at other wavelengths over a 25-yr period reveals correlated flux variations from radio to X-ray wavelengths. We interpret the variable radio to optical emission as synchrotron radiation, self-absorbed in the radio/millimetre region, and the X-rays mainly as a result of Compton up-scattering of low-energy photons by the population of high-energy electrons that give rise to the synchrotron radiation.

Key words: accretion, accretion discs – galaxies: active – galaxies: nuclei – quasars: general – quasars: individual: III Zw 2.

1 INTRODUCTION

Active galactic nuclei (AGN) are luminous objects thought to be powered by accretion of material on to a supermassive black hole. They emit radiation across a wide frequency range from γ-ray to radio wavelengths. X-ray emission, relativistic jets and superluminal motion are phenomena that originate close to the central power source and can be used to study conditions in innermost regions around the black hole. Correlation and lags in variability at different wavelengths allow us to discriminate between theoretical models that explain energy generation close to the central source.

III Zw 2 is a triple galaxy group. The brightest of the group, III Zw 2A (Mrk 1501, PG 0007+106) is an AGN with a Seyfert 1 nucleus and will be referred to as III Zw 2 throughout this paper. III Zw 2 is a bright X-ray source ($F_{0.2-10} \approx 4 \times 10^{-11}$ erg cm^{-2} s^{-1}, Schnopper et al. 1978) with $z = 0.089$ (de Robertis 1985) and is the most luminous Seyfert I in the sample of Piccinotti et al. (1982) ($L_{2-10} \approx 10^{45}$ erg s^{-1}). Superluminal motion of a radio-emitting plasma has been observed recently in the source; notably this is the first detection of its kind in a spiral galaxy (Brunthaler et al. 2000). III Zw 2 has long been known to show large-amplitude flux variations in the radio (Wright et al. 1977; Schnopper et al. 1978; Landau, Epstein & Rather 1980; Aller et al. 1985; Falcke et al. 1999) and the optical bands (Lloyd 1984; Clements et al. 1995). Variations of smaller amplitude (of less than 50 per cent), have also been detected in the infrared (IR) (Lebofsky & Rieke 1980; Sembay, Hanson & Coe 1987) and the ultraviolet (UV) (Chapman, Geller & Huchra 1985). The X-ray temporal behaviour is less well studied,

⋆E-mail: njs@mssl.ucl.ac.uk

but comparison of observations at different epochs hints that the X-ray flux may vary substantially. The X-ray spectra of III Zw 2 obtained by *SAS-3* (Schnopper et al. 1978), *Ariel VI* (Hall et al. 1981) and the *Einstein* SSS (Petre et al. 1984), can be described by power laws with photon indices $\Gamma = 1.3$–1.7, and neutral absorption consistent with that of the line-of-sight Galactic column density. No soft X-ray excess has been detected in the source.

In this paper we study the X-ray to radio emission in III Zw 2 over a period of 25 yr, from 1975 to 2000. We discuss the different X-ray observations, starting with the most recent *XMM–Newton* observation in 2000 July and going back to the *SAS-3* observation of 1977. We present an analysis of the X-ray spectra of III Zw 2 taken by four different observatories and examine the short- and long-term temporal variations in X-ray flux (Section 2). We also present the multiwavelength light curves and spectral energy distribution (SED) incorporating data from 1975 to 2000 (Section 3) and discuss the emission mechanisms in the source (Section 4).

2 X-RAY EMISSION

2.1 Observations

III Zw 2 has been observed in the X-ray band 15 times during the last three decades (see Table 1 for details). To build up a reliable X-ray history for this source we have only considered data with good positional resolution, i.e. data taken with an imaging telescope or the *SAS-3* Rotating Modulation Collimator (RMC). This is because of the presence of a bright X-ray source, HD 560, approximately 12 arcmin from III Zw 2. This source may have been responsible for the contamination of the non-imaging *EXOSAT* ME flux measurements of III Zw 2 in 1985 (Tagliaferri et al. 1988).

2.1.1 XMM–Newton

III Zw 2 was observed with *XMM–Newton* (Jansen et al. 2001) on 2000 July 4. The observatory has two types of X-ray instruments on board: the European Photon Imaging Camera (EPIC) (Strüder et al. 2001; Turner et al. 2000) which is made up of three charge-coupled device (CCD) cameras (MOS1, MOS2, PN) and the dispersive Reflection Grating Spectrometer (RGS) for high-resolution spectroscopy (den Herder et al. 2001). MOS data were taken in the full frame mode while the PN data were taken in small window mode. Thin filters were used in all three EPIC cameras.

EPIC data were reduced using the *XMM–Newton* Standard Analysis Software (SAS), version 5.2. Source spectra and light curves from the MOS and PN detectors were extracted using circles of radius 2 arcmin with pattern 0–12 (MOS) and 50 arcsec with pattern 0 (PN) in XMMSELECT. The background spectra and light curves were extracted using circular apertures from a source-free region on the same chip.

RGS data were reduced using *XMM–Newton* SAS V5.0.1. Source spectra were extracted from a spatial region containing 90 per cent of the source flux in the cross-dispersion direction. The first and second orders were selected from pulse height–dispersion regions containing 95 per cent of the source counts. Background spectra were obtained using the same order-sorting regions as for the source, but spatial regions excluding 95 per cent of the source flux in the cross-dispersion direction. First- and second-order background-subtracted spectra from RGS1 and RGS2 were resampled to match the first-order RGS1 spectrum and added together. The corresponding response matrices were divided by the data/model ratio of a power-law fit to the RGS spectra of the continuum source Mrk 421 to correct systematic residuals in the effective area calibration. The response matrices were then resampled and combined into a single response matrix. Finally, the RGS spectrum was grouped by a factor of 10 to improve the signal-to-noise ratio.

2.1.2 Archival data

Archival data from the *ASCA*, *ROSAT*, *EXOSAT* and *Einstein* satellites were also included in this study. The XSELECT software was used to generate all spectra and light curves. Background spectra and light curves were extracted from source-free regions using circular apertures.

Table 1. X-ray observations of III Zw 2 over a period of 25 yr, from 1975 to 2000. The 1–2 keV model flux has been obtained from power-law spectral fits. For data with no spectral information, count rates have been converted to flux via the PIMMS flux converter assuming a power-law spectral model using $\Gamma = 1.7$ and $N_{\rm H} = 5.72 \times 10^{20}$ cm^{-2}.

Date	Instrument	Energy range	Spectra	Exposure (s)	Count rate	Flux 1–2 keV (erg cm^{-2} s^{-1})
2000 July 4	*XMM–Newton* MOS	0.1–10.0	Y	7500	1.078	1.910e−12
	XMM–Newton PN	0.1–10.0	Y	10 152	2.740	1.910e−12
	XMM–Newton RGS	0.3–2.3	Y	16 000	0.119	1.830e−12
1997 July 1	*ASCA* SIS	0.4–10.0	Y	40 352	0.41	3.100e−12
	ASCA GIS	0.7–10.0	Y	43 744	0.360	3.100e−12
1994 December 26	*ROSAT* HRI	0.1–2.0	N	2605	0.089	1.460e−12
1994 June 16	*ROSAT* HRI	0.1–2.0	N	1601	0.205	3.370e−12
1992 July 18	*ROSAT* PSPC	0.1–2.0	Y	9013	0.288	1.800e−12
1992 June 12	*ROSAT* PSPC	0.1–2.0	Y	9111	0.314	1.960e−12
1990 December 22	*ROSAT* PSPC	0.1–2.0	N	563	0.480	2.840e−12
1985 December 20	*EXOSAT* LE ($L \times 3$)	0.05–2.0	N	14 948	0.036	1.080e−11
1985 November 30	*EXOSAT* LE ($L \times 3$)	0.05–2.0	N	16 655	0.028	8.370e−12
1985 August 18	*EXOSAT* LE ($L \times 3$)	0.05–2.0	N	5847	0.038	1.136e−11
1983 December 18	*EXOSAT* LE ($L \times 3$)	0.05–2.0	N	4521	0.013	3.887e−12
1980 December 19	*Einstein* IPC	0.4–4.0	Y	4233	0.077	7.950e−13
1980 January 9	*Einstein* IPC	0.4–4.0	Y	3270	0.365	2.960e−12
1979 June 21	*Einstein* IPC	0.4–4.0	Y	805	0.772	6.210e−12
1977 August 17–22	*SAS-3* (RMC)	2.0–11.0	N	–	–	7.580e−12

The *ASCA* (Inoue 1993), Gas Imaging Spectrometer (GIS, hereafter GIS2 and GIS3) data in high bit rate mode and the Solid-state Imaging Spectrometer (SIS, hereafter SIS0 and SIS1) data in bright2 mode were screened using ASCASCREEN by applying the standard screening criteria. FTOOLS were used to apply dead-time correction and to generate the response matrices. Source spectra and light curves were extracted using a circle of 6-arcmin radius.

We analysed data from the *ROSAT* Position Sensitive Proportional Counter (PSPC) (Briel et al. 1988; Pfeffermann et al. 1987), which was an imaging spectrometer and the High Resolution Imager (HRI) (Harris, Stern & Biretta 1990). Spectra and light curves were extracted from the PSPC data using a source circle of 2 arcmin. The All-sky Survey (Voges et al. 1999) count rate of 1990 December 22 was obtained from the *ROSAT* archives. The HRI data have no useful energy resolution but have a spatial resolution of ∼5 arcsec and were used to generate source and background light curves using a circle of 1.3-arcmin radius.

EXOSAT observations of III Zw 2 were made using both the low-energy (LE) and the medium-energy (ME) detectors (Andrews 1984; Bleeker 1975; Turner, Smith & Zimmermann 1981). For our analysis, we have used the LE imaging Channel Multiplier Array (CMA) data. Count rates for the LX3 filter exposures were determined using a circle of 1.5-arcmin radius.

Spectra and light curves from the *Einstein* Imaging Proportional Counter (IPC), which was sensitive to the 0.4–4.0 keV range were extracted from screened event lists using a circle of 1-arcmin radius.

The X-ray flux for the *SAS-3* observation is taken from Schnopper et al. (1978). The *SAS-3* 90 per cent error circle on the position of III Zw 2 has a radius of 40 arcsec. This uncertainty is small enough to safely exclude the possibility of flux contamination of III Zw 2 from the X-ray source 12-arcmin away.

2.2 X-ray spectra

Spectral fitting of X-ray data was done using the XSPEC software package version 11.1. All emission-line energies quoted in the text are in the rest frame of the source and errors are quoted at the 90 per cent confidence level unless specified otherwise. Spectral fitting results are summarized in Table 2.

2.2.1 XMM–Newton

The MOS and PN spectra were grouped to a minimum of 35 and 70 counts per bin, respectively, and fitted over an energy range of 0.3–10.0 keV.

Initially we fitted the MOS1, MOS2 and PN spectra individually with a power law and neutral absorption. This gives a photon index of $\Gamma = 1.66 \pm 0.03$ and $N_{\rm H} = 4.50^{+1.29}_{-1.25} \times 10^{20}$ cm^{-2} for the MOS1 spectrum (χ^2/dof = 175/156), $\Gamma = 1.69 \pm 0.03$ and $N_{\rm H} = 4.43^{+1.29}_{-1.08} \times 10^{20}$ cm^{-2} for the MOS2 spectrum (χ^2/dof = 199/157) and $\Gamma = 1.76 \pm 0.03$ and $N_{\rm H} = 5.53^{+0.53}_{-0.47} \times 10^{20}$ cm^{-2} for the PN spectrum (χ^2/dof = 367/281). The fitted absorption column density is consistent with that expected from the Galactic ISM along the line of sight to III Zw 2 ($N_{\rm H} = 5.72 \times 10^{20}$ cm^{-2}). To investigate the presence of absorption over and above the Galactic column we added another neutral column in the rest frame of the source. This did not significantly improve the fit. We find upper limits on the absorption intrinsic in III Zw 2 of $N_{\rm H} < 2.30 \times 10^{20}$, 3.54×10^{20} and 1.04×10^{20} cm^{-2} at a 90 per cent confidence level for MOS1, MOS2 and PN, respectively. Addition of a blackbody soft excess component to the power-law model makes no improvement to the fit in either the MOS or PN spectra.

Residuals with respect to the power-law fit show an excess of between 5.5 and 7.5 keV in both MOS and PN spectra, probably as a result of the presence of an Fe Kα line. To account for these residuals we added a single Gaussian to the underlying power law, keeping the absorption fixed to the Galactic value. This yields a broad line with the energy centred at $E = 6.67 \pm 0.40$ keV in MOS1 ($\sigma = 1.10\pm$, χ^2/dof = 163/154), at $E = 6.82 \pm 0.29$ keV in MOS2 ($\sigma = 1.20 \pm 0.35$ keV, χ^2/dof = 176/155) and at $E = 6.24 \pm 0.25$ keV in PN ($\sigma = 1.37 \pm 0.29$ keV, χ^2/dof = 314/279).

To better constrain the fit we fitted the same model to the MOS and the PN spectra simultaneously. Hereafter, the neutral absorption was fixed at the Galactic value of $N_{\rm H} = 5.72 \times 10^{20}$ cm^{-2} for all spectral

Table 2. The Galactic column is fixed at $N_{\rm H} = 5.72 \times 10^{20}$ cm^{-2} for all spectral fits.

Date	Model	Γ	Power-law norm	Line				χ^2/dof
				Energy (keV)	σ (keV)	EW (keV)	Incl.	
			XMM–Newton (MOS1+MOS2+PN)					
2000 July 4	PL	1.75±0.01	1.67e−3±0.34e−4	–	–	–	–	764/598
	PL+Gau	1.79±0.01	1.67e−3±0.34e−4	6.44±0.35	1.25±0.35	$1.25^{+0.31}_{-0.35}$	–	680/595
	PL+disc–line[a]	1.79±0.01	1.67e−3±0.34e−4	$5.95^{+0.45}_{-0.14}$	–	$0.96^{+0.24}_{-0.18}$	$88^{\circ+2}_{-15}$	685/594
	PL+disc–line[b]	1.77±0.01	1.67e−3±0.34e−4	$7.63^{+0.63}_{-0.58}$	–	$0.82^{+0.07}_{-0.20}$	$25^{\circ+8.0}_{-7.6}$	694/594
	Pexrav+Gau[b]	1.79±0.01	1.66e−3±0.34e−4	6.45±0.35	1.40±0.60	$0.87^{+0.73}_{-0.47}$	10°	677/593
	Pexriv+Gau[b]	1.79±0.01	1.66e−3±0.34e−4	6.49±0.44	1.22±0.74	$0.88^{+0.52}_{-0.38}$	9°	677/592
			ASCA (GIS2+GIS3+SIS0+SIS1)					
1997 July01	PL	1.72±0.02	2.71e−3±0.74e−4	–	–	–	–	620/599
	PL+GAU	1.75±0.02	2.75e−3±0.79e−4	6.72±0.26	0.83±0.33	$0.40^{+7.60}_{-0.24}$	–	604/596
			ROSAT (PSPC)					
1992 July 18	PL	1.61±0.08	1.54e−3±0.56e−4	–	–	–	–	79/58
1992 June 12	PL	1.52±0.06	1.59e−3±0.56e−4	–	–	–	–	70/63
			Einstein (IPC)					
1979 June 21	PL	2.06±0.30	6.07e−3±0.43e−3	–	–	–	–	13/5
1980 January 9	PL	2.26±0.27	3.18e−3±0.19e−3	–	–	–	–	6/6
1980 December 19	PL	1.91±0.40	7.56e−4±1.1e−4	–	–	–	–	4/5

[a]Disc inclination free to vary. [b]Disc inclination constrained between 0° and 40°.

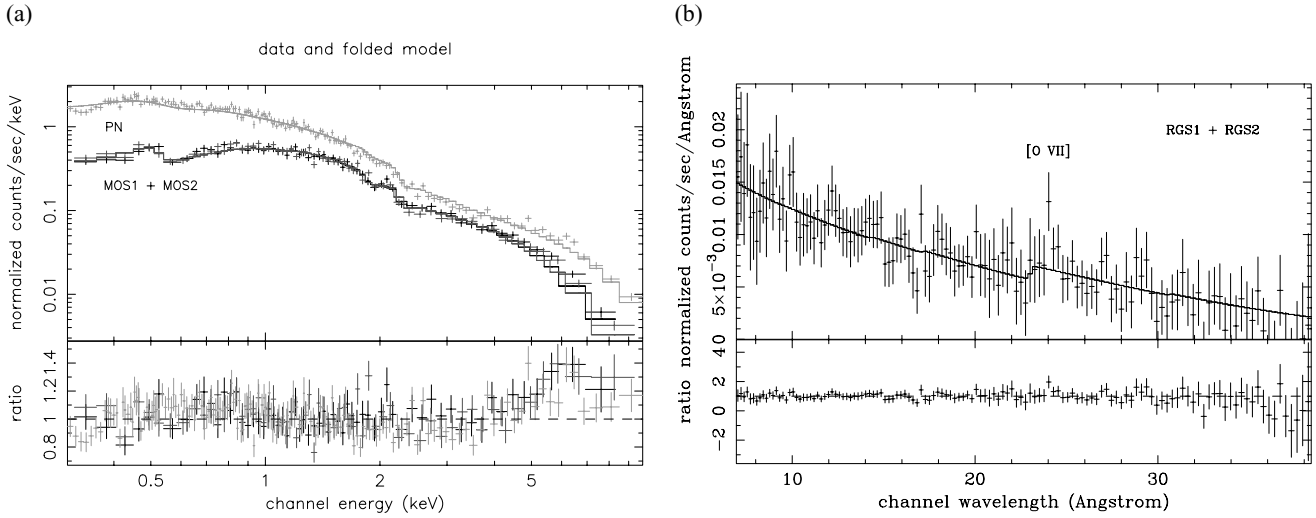

Figure 1. Left: simultaneous power-law fit to the MOS1, MOS2 and PN data ($\Gamma = 1.75 \pm 0.01$, $\chi^2/\mathrm{dof} = 764/598$). The data have been plotted with a signal-to-noise ratio of 10. Right: power-law fit to the RGS data ($\Gamma = 1.61 \pm 0.12$, $\chi^2/\mathrm{dof} = 65/129$). The Galactic column is fixed at $N_{\mathrm{H}} = 5.72 \times 10^{20}$ cm^{-2} for both spectral fits.

fitting. The simultaneous power-law fit gives a photon index of $\Gamma = 1.75 \pm 0.01$ ($\chi^2/\mathrm{dof} = 764/598$). Residuals with respect to the power-law fit again show a broad feature between 5.5 and 7.5 keV (Fig. 1). The addition of a single broad Gaussian to the underlying power law yields a line at $E = 6.44 \pm 0.35$ keV ($\sigma = 1.25 \pm 0.35$, equivalent width, $\mathrm{EW} = 1.25^{+0.31}_{-0.35}$ keV) and makes a significant improvement to the fit ($>4\sigma$) with $\chi^2/\mathrm{dof} = 680/595$ ($\Delta\chi^2 = 84$ for three extra parameters).

One model for the broad line emission at around 6.4 keV is fluorescence Fe Kα originating in an accretion disc around a central black hole. We thus fitted the excess between 5.5 and 7.5 keV, with a 'disk line' model (Fabian et al. 1989), for an accretion disc around a Schwarzschild black hole. Adding this component (with fixed $R_{\mathrm{in}} = 6R_{\mathrm{s}}$ and $R_{\mathrm{out}} = 1000R_{\mathrm{s}}$) to the underlying power law with line energy, inclination and emissivity free to vary, yields a line at $E = 5.95^{+0.45}_{-0.14}$ keV ($\mathrm{EW} = 0.96^{+0.24}_{-0.18}$ keV) for a high inclination of $88^{+2}_{-15}{}^{\circ}$ and emissivity (q) $= -3.07 \pm 0.35$ (where the emissivity varies as R^q). The goodness of fit ($\chi^{2/\mathrm{dof}} = 685/594$, $\Delta\chi^2 = 79$ for four extra parameters) is comparable with that of the broad Gaussian model. The best-fitting inclination of $\approx 90^{\circ}$ conflicts, however, with the observation of superluminal motion in the source, which implies an inclination in the range of 0°–40° for the radio jet (Brunthaler et al. 2000). With the inclination restricted to $\leqslant 40^{\circ}$ the disc–line model yields a line at $7.63^{+0.63}_{-0.58}$ keV ($\mathrm{EW} = 0.81^{+0.07}_{-0.20}$ keV) with $q = -5.54 \pm 1.44$, inclination $25^{+8.0}_{-7.6}{}^{\circ}$ and the overall fit statistic of $\chi^2/\mathrm{dof} = 694/594$.

We also fitted the excess between 5.5 and 7.5 keV, with a 'Laor' model (Laor 1991), for a disc around a rotating black hole. A power-law and Laor line model (inclination $\leqslant 40^{\circ}$ and emissivity free to vary), yields a line at $8.60^{+1.00}_{-0.70}$ keV ($\mathrm{EW} = 1460^{+870}_{-800}$ keV) with $q = 3.77 \pm 0.36$, inclination $= 21^{+40}_{-21}{}^{\circ}$ and an overall fit statistic of $\chi^2/\mathrm{dof} = 689/593$.

We checked for the presence of an iron edge at $E > 7$ keV. The addition of an edge to the underlying power law, with the energy of the edge constrained between 7 and 9 keV, makes no improvement to the fit ($\Delta\chi^2 = 0$). A model consisting of a power law plus a reflection component from either neutral (pexrav model) or ionized matter (pexriv model) is a significantly better fit than only a power-law model ($\Delta\chi^2 = 60$ and $\Delta\chi^2 = 71$ for neutral and ionized matter, respectively, for three extra parameters). The reflection component is strong with $R = 1.82^{+0.87}_{-0.70}$, where R is the solid angle subtended by the reflecting material in steradians.

Adding a Gaussian to the pexrav and pexriv model yields a broad line at 6.45 ± 0.35 keV ($\sigma = 1.24 \pm 0.60$ keV, $\mathrm{EW} = 872^{+0.73}_{-0.47}$ eV, $\Delta\chi^2 = 27$ for three extra parameters) and 6.49 ± 0.44 keV ($\sigma = 1.22 \pm 0.74$ keV, $\mathrm{EW} = 880^{+0.52}_{-0.38}$ eV, $\Delta\chi^2 = 17$ for three extra parameters), respectively. The addition of a Gaussian improves the goodness of the fit at greater than 99.99 per cent confidence level for both neutral and ionized reflection. Replacing the Gaussian with a disc–line (with inclination restricted to $\leqslant 40^{\circ}$) yields a line at 7.84 ± 0.40 and 7.94 ± 0.90 keV for the pexrav and pexriv model, respectively.

Apart from the Fe emission the EPIC spectra are apparently featureless. The higher-resolution RGS spectrum can be described by a power law of $\Gamma = 1.61 \pm 0.12$ with neutral absorption corresponding to the Galactic column ($\chi^2/\mathrm{dof} = 65/129$), which is consistent with the EPIC spectra. Although the χ^2 value is very low owing to the relatively low signal-to-noise ratio of the spectrum, the largest residual (2σ) is seen at 22.08 ± 0.015 Å in the rest frame of the source, which is consistent with forbidden [O VII] line emission.

2.2.2 *Archival spectra*

The *ASCA* GIS and SIS data were grouped to give a minimum of 35 counts per bin. SIS data below 1.0 keV were ignored owing to a decrease in efficiency below that energy for observations after 1994, which is not corrected for by the current software for generating response matrices. A power-law fit to all the data (energy range of 0.7–10.0 keV for GIS and 1.0–10.0 keV for SIS) gives a photon index $\Gamma = 1.72 \pm 0.02$ ($\chi^2/\mathrm{dof} = 620/599$) consistent with the *XMM* observation (Fig. 2). The addition of a broad Gaussian to the underlying power law yields a line at $E = 6.72 \pm 0.26$ ($\sigma = 0.83 \pm 0.33$ keV, $\Delta\chi^2 = 16$ for three extra parameters) making a $>3\sigma$ improvement over the power-law fit ($\chi^2/\mathrm{dof} = 604/596$). The line has an equivalent width of $\mathrm{EW} = 0.43^{+7.6}_{-0.24}$ keV and a velocity width with $\mathrm{FWHM} = 87\,000$ km s^{-1}. Just as in the *XMM* observation, there is

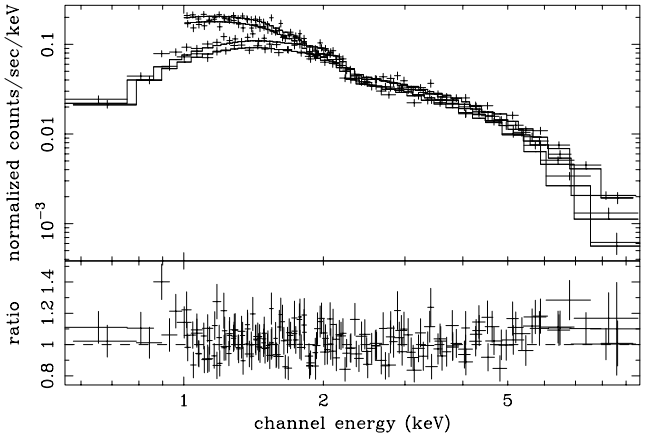

Figure 2. Simultaneous power-law fit to the SIS and GIS data ($\Gamma = 1.72 \pm 0.02$, $\chi^2/\mathrm{dof} = 620/599$). The data are plotted with a signal-to-noise ratio of 10. The Galactic column is fixed at $N_\mathrm{H} = 5.72 \times 10^{20}$ cm^{-2}.

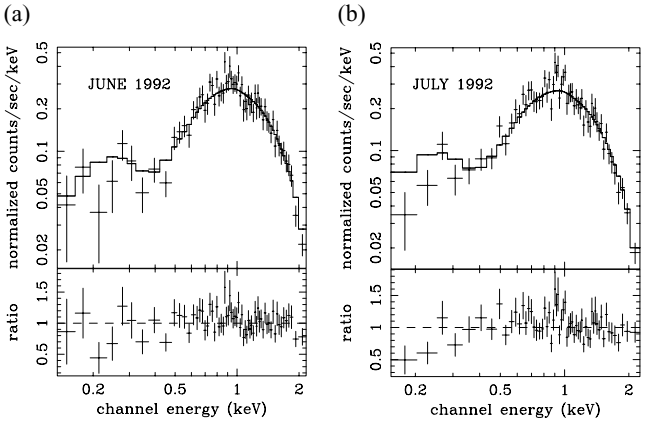

Figure 3. Left: power-law fit to the *ROSAT* June spectrum ($\Gamma = 1.52 \pm 0.06$, $\chi^2/\mathrm{dof} = 70/63$). Right: power-law fit to the *ROSAT* July spectrum ($\Gamma = 1.61 \pm 0.08$, $\chi^2/\mathrm{dof} = 79/58$). The Galactic column is fixed at $N_\mathrm{H} = 5.72 \times 10^{20}$ cm^{-2}).

no evidence of intrinsic absorption or of an excess at the soft X-ray end of the spectrum.

Spectra from the 1992 *ROSAT* PSPC observations were grouped to give a minimum of 35 counts per bin. Both spectra are essentially featureless (Fig. 3) and can be described by a power law and a Galactic column similar to the previous observations. Spectral fitting in the energy range of 0.1–2.0 keV results in a photon index $\Gamma = 1.52 \pm 0.06$ for the June spectrum ($\chi^2/\mathrm{dof} = 70/63$) and $\Gamma = 1.61 \pm 0.08$ for the July spectrum ($\chi^2/\mathrm{dof} = 79/58$). There is no significant intrinsic absorption over and above the Galactic column or an excess at softer energies, consistent with results from the *ASCA* and *XMM* observations.

Spectra obtained from the Einstein IPC were grouped to a minimum of 20 counts per bin and fitted in the energy range of 0.4–4.0 keV (see Fig. 4). The 1980 December spectrum can be well described by a single power law of $\Gamma = 1.91 \pm 0.40 (\chi^2/\mathrm{dof} = 4/5)$. A power-law fit to the 1980 January and 1979 June spectra gives a photon index $\Gamma = 2.26 \pm 0.27 (\chi^2/\mathrm{dof} = 6/6)$ and $\Gamma = 2.06 \pm 0.30 (\chi^2/\mathrm{dof} = 13/5)$, respectively. We caution that there are large uncertainties in the IPC response matrices and the data are of low signal-to-noise ratio.

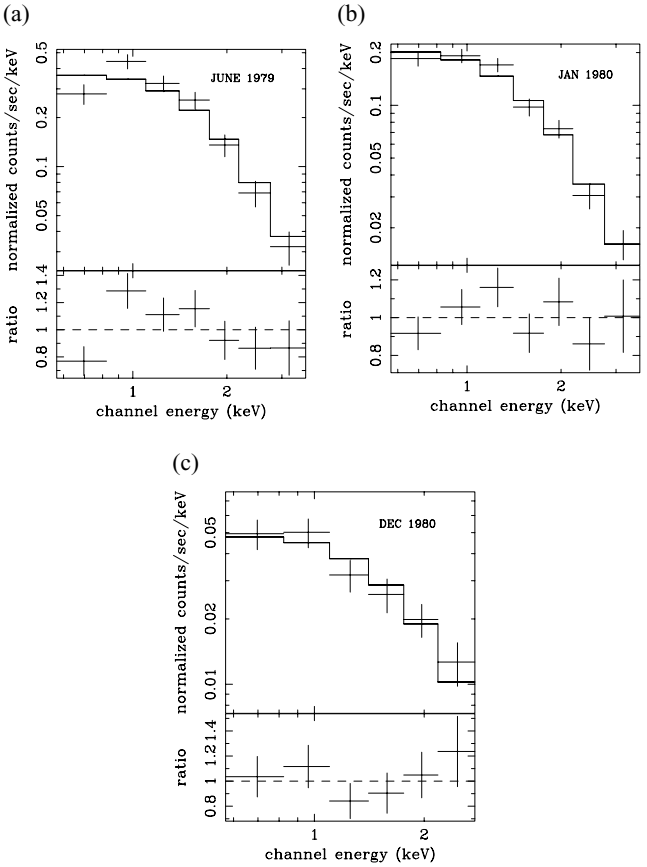

Figure 4. *Einstein* IPC spectra: 1979 June ($\Gamma = 2.06 \pm 0.30$, $\chi^2/\mathrm{dof} = 13/5$), 1980 January ($\Gamma = 2.26 \pm 0.27$, $\chi^2/\mathrm{dof} = 6/6$), 1980 December ($\Gamma = 1.91 \pm 0.40$, $\chi^2/\mathrm{dof} = 4/5$).

2.3 X-ray variability

Light curves from observations between 1975–2000 were compiled to study short-term variability of the source. No significant flux variations are observed during any of the observations. Fig. 5 shows typical light curves from different observatories. We performed statistical analysis for each time series to determine the constant source probability associated with the χ^2 value. Results of the analysis are listed in Table 3 and confirm the absence of significant X-ray variability in any of the observations that probed time-scales between 100 and 45 000 s.

To study long-term X-ray behaviour of the source we determined the 1–2 keV flux for each observation. Model flux for data with spectral information were obtained directly from spectral fits. For other observations broad-band count rates were converted to an equivalent flux in the 1–2 keV band using the PIMMS flux converter, assuming a power-law spectral model. As the spectral photon indices and neutral absorption are similar in the *XMM* observation and in previous X-ray observations (e.g. Hall et al. 1981; Petre et al. 1984), we have used the power-law index $\Gamma = 1.7$ (deduced from the *XMM*-EPIC data) and $N_\mathrm{H} = 5.72 \times 10^{20}$ cm^{-2} for conversion. The 1–2 keV flux for *SAS-3* was determined (assuming a power-law spectral model) using the 1–10 keV flux and the best-fitting photon index $\Gamma = 1.3$ from Schnopper et al. (1978). Fig. 6 shows the 1–2 keV flux variations in III Zw 2. The light curve shows 10-fold flux variations, over time-scales of years.

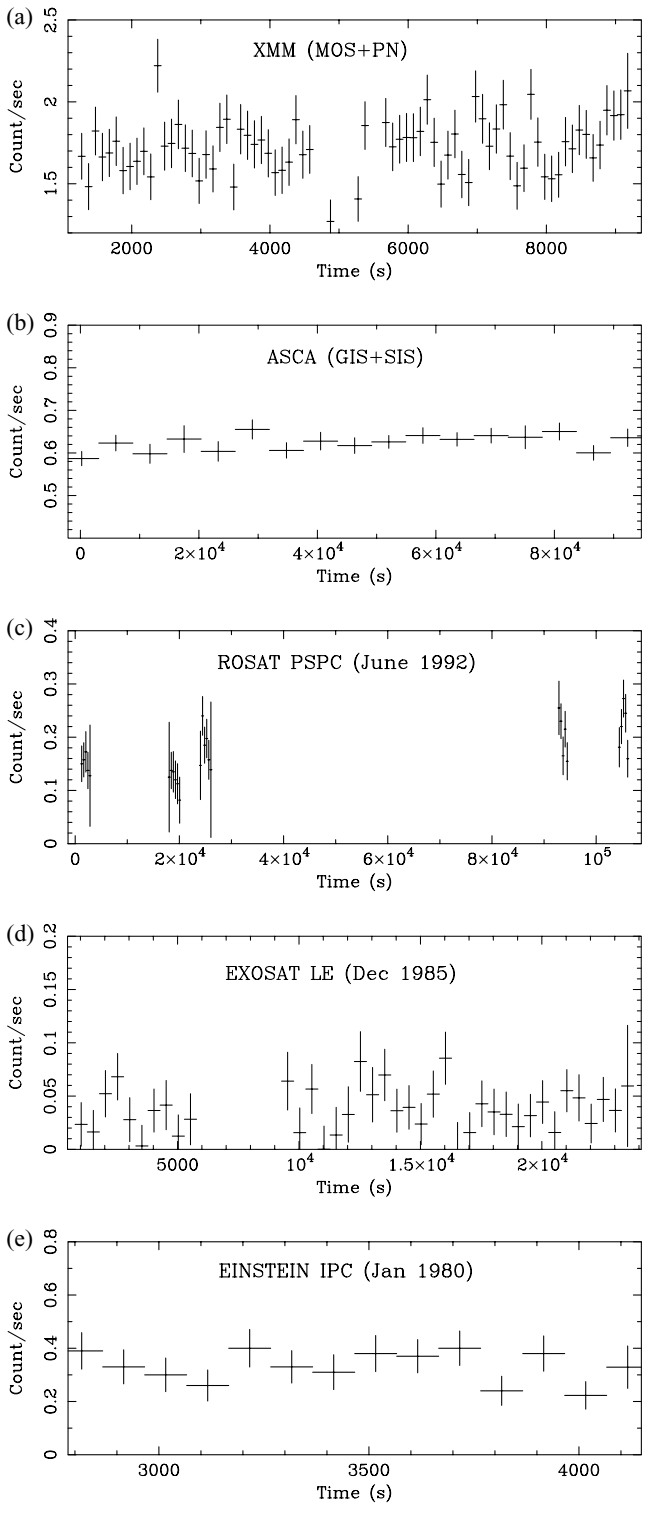

Figure 5. Typical light curves of III Zw 2 from different observatories.

3 MULTIWAVELENGTH EMISSION

All available data at UV, optical, infrared and radio wavelengths from 1975 to 2000 were obtained from archives, the literature and other sources. These data were combined along with the X-ray data to study the long-term behaviour of the source over a broad spectral range.

Table 3. Results of the statistical test to determine the constancy of light curves for the different missions. There is no significant variation in X-ray flux of III Zw 2 during any of the observations.

Mission	Date	Bin time (s)	χ^2/dof	Prob. of constancy
XMM–MOS	2000 July 4	100	27/29	0.54
ASCA	1997 July 1	5760	15/16	0.52
ROSAT	1994 December 26	400	2/6	0.87
	1994 June 16	400	4/3	0.29
	1992 July 18	400	6/18	0.99
	1992 June 12	400	25/26	0.48
EXOSAT	1985 December 20	100	170/187	0.98
	1985 November 30	100	174/215	0.98
	1985 August 18	100	76/85	0.74
	1983 December 18	100	40/48	0.80
Einstein	1980 January 9	100	4/12	0.98
	1980 December 19	100	27/36	0.85
	1979 June 21	100	6/8	0.64

3.1 Multiwavelength data

Ultraviolet data are from the *IUE* archives (Chapman et al. 1985). Optical *B*-band data from 1975 to 1991 are a combination of photometry from different photographic monitoring experiments. Data from 1975 to mid 1977 were taken from Lloyd (1984) and data from mid 1977–1991 are from Clements et al. (1995). The CCD photometry data for 1989, 1992 and 1998 were obtained from the LaPalma ING (Issaac Newton group of telescopes) archives.

The infrared data of 2000 October are from the SAAO and the rest are compiled from various publications listed below: 1975 December and 1978 January (Rieke & Lebofsky 1979), 1985 September (Elvis et al. 1994), 1977 July (Neugebauer et al. 1979), 1978 June (Condon et al. 1981), 1979 August (McAlary et al. 1983), 1977 November (Hyland & Allen 1982), 1983 June (Edelson & Malkan 1987), (Lebofsky & Rieke 1980) and 1988 October to 1989 September (Kotilainen et al. 1992). The 1998 May/June millimetre data were obtained from the JCMT archives and the rest from Landau et al. (1980). The radio data at 22 and 37 GHz are from Metsähovi (see Teräsranta et al. 1998) and at 14.5 and 8 GHz are from Michigan.

3.1.1 Data reduction

Optical images from the Isaac Newton Telescope (INT, 2.5 m) and the Jacobus Kapteyn Telescope (JKT, 1.0 m) of the ING archives were used to obtain magnitudes for III Zw 2 via differential photometry. The instrumental magnitudes were extracted from the images via aperture photometry using the GAIA software. *UBVRI* zero-points were determined using the standard stars LA97284 (JKT) and 95Z96 (INT). For those images not accompanied by standard star observations magnitudes for III Zw 2 were obtained via differential photometry using the calibrated magnitudes of other stars in the III Zw 2 field. The *UBVRI* magnitudes for III Zw 2 were corrected for extinction using the airmass and atmospheric extinction measured at LaPalma for the individual days. Systematic errors have been added using the scatter in magnitude of other stars in the III Zw 2 field of view. Magnitudes were converted to flux using the relation $f = 4.39 \times 10^6\,(10^{-0.4M})$ mJy (Clements et al. 1995). An additional 10 per cent error was included to account for the systematic differences between the photographic and CCD measurements.

J, *H* and *K* photometric observations were made with the MkII Infrared Photometer on the 1.9-m telescope at the SAAO in

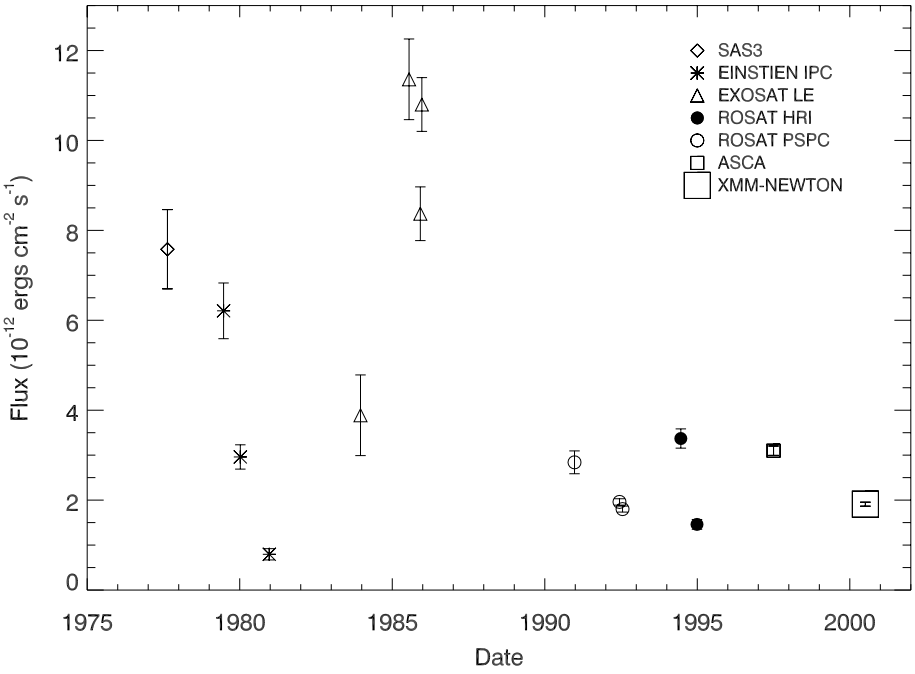

Figure 6. X-ray (1–2 keV) light curve of III Zw 2 from 1975 to 2000. Model flux for data with spectral information was obtained directly from spectral fits [*XMM*, *ASCA*, *ROSAT* (1992) and *Einstein*]. For other observations, broad-band count-rates were converted to equivalent flux in the 1–2 keV band using the PIMMS converter (assuming a power-law model with a photon index $\Gamma = 1.7$, $N_{\rm H} = 5.72 \times 10^{20}$ cm^{-2}). The *SAS-3* flux was determined via PIMMS (assuming a power-law spectral model) using the 1–10 keV flux and the best-fitting photon index $\Gamma = 1.3$ from Schnopper et al. (1978).

Sutherland. These data were reduced to the current standard SAAO photometric system (Carter 1990) using standard SAAO IR photometry reduction software. Each observation was then corrected to a nearby standard from the Carter (1990) list.

Data from the James Clerk Maxwell Telescope (JCMT) archives were taken with the Submillimetre Common User Bolometer Array (SCUBA; Holland et al. 1999). SCUBA was used in photometry mode to make observations at 2000, 1350 and 850 μm. These observations were retrieved from the JCMT archive and reduced in the standard manner. At 850 μm the off-source bolometers were used to remove correlated sky noise from the source signal. Flux calibration was made with respect to either Uranus or the JCMT secondary calibrator CRL2688.

3.2 Multiwavelength emission

3.2.1 Variability

Multiwavelength emission from X-ray to radio wavelengths for III Zw 2 over a period of 25 yr from 1975 to 2000 is presented in Fig. 7. The radio and optical (up to 1990) wavelengths are better sampled than the other bands. The source shows 10- and 20-fold variations in the X-ray and radio bands, respectively. The amplitude of variations is somewhat smaller in the optical (fourfold) and IR (twofold). Visual inspection of the multiband light curves shows related behaviour from X-ray to radio wavelengths. The X-ray and the optical bands appear to be coincident in time, but the radio flux is seen to peak later (a lag of about 13 months between the optical and 8-GHz emission has been reported by Clements et al. 1995).

We performed a Pearson linear correlation test to determine correlation, if any between X-ray, UV, optical and IR emission. Except for the optical the other wavelengths are not very well sampled and hence we used a simple approach. The optical light curve was interpolated and was used to determine the optical flux corresponding to the individual X-ray, UV and IR flux points. The Pearson linear correlation coefficient for different wavelengths is listed in Table 4. The X-ray band is found to be significantly correlated with the optical band ($>3\sigma$). The correlation of light curves at the UV and IR wavelengths is less significant ($>2\sigma$).

3.2.2 Spectral energy distribution

Fig. 8 shows the total spectral energy distribution of III Zw 2, incorporating data from 1975 to 2001. The lack of spread in data in the frequency range 10^{11}–10^{14} Hz is probably a result of fewer observations in that region. The spectrum peaks at the optical/IR wavelengths, with no evidence for an excess in UV and soft X-ray wavelengths. The overall spectral energy distribution shows a power law over a broad frequency range (10^{11}–10^{14} Hz). A change in power-law gradient (hardening) is observed below 10^{11} Hz. The SED would have to be steeper between 10^{15} and 10^{16} Hz than at lower frequencies in order for the UV and to connect with the X-ray band. Above 10^{16} Hz the spectrum becomes hard again.

4 DISCUSSION

4.1 X-ray emission

A study of the *XMM*, *ASCA* and *ROSAT* X-ray spectra reveals that there is relatively little change in the power-law photon index ($\Gamma \approx$ 1.6–1.8) between 1992 and 2000. Spectra obtained from the *Einstein* IPC (with the exception of 1980 January) and previous missions such as *Ariel VI* (Hall et al. 1981) and *SAS-3* can also be described, within errors by $\Gamma \approx 1.6$–1.8.

A power-law slope of $\Gamma \approx 1.7$ is typical of Seyfert 1 galaxies (Reynolds 1997; Green, McHardy & Lehto 1993). Current models

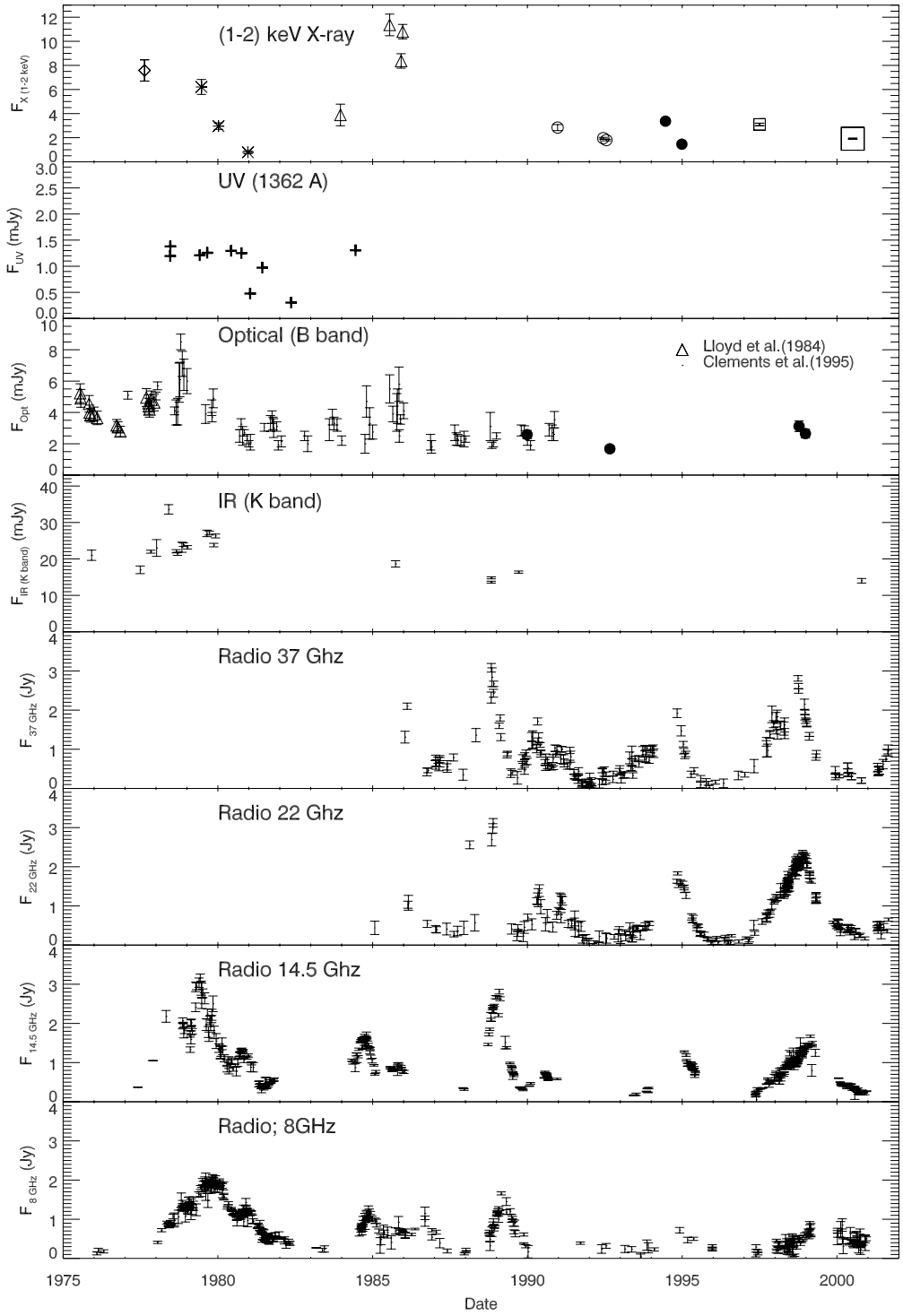

Figure 7. Multiwavelength light curves of III Zw 2 showing flux variations, with increasing wavelengths from top to bottom. (See Section 3 for the sources of data.)

for the production of the X-ray continuum explain these spectroscopic observations by the presence of a hot Comptonizing corona or an electron–positron pair corona that up-scatters thermal soft photons from the accretion disc to generate the hard X-ray power law (e.g. Haardt, Maraschi & Ghisellini 1994). A power-law slope of $\Gamma \approx 1.7$ is also typically observed for synchrotron radiation in radio sources (Kukula et al. 1998; Bloom et al. 1999). III Zw 2 is a strong radio source with relativistic jets and therefore it is possible that synchrotron or synchrotron self-Compton eadiation makes a significant contribution to the X-ray continuum. Thus, on its own the power-law slope does not allow us to distinguish between the possible origins for the X-ray continuum.

A soft X-ray excess is common amongst quasars (Wilkes et al. 1989; Masnou et al. 1992; Saxton et al. 1993) and Seyfert I galaxies

Table 4. The table gives the Pearson linear correlation coefficient and probability that there is no linear correlation between the light curves at these wavelengths.

Wavelengths	Coefficient (r)	Probability
X-ray/opt	0.86	0.00072
UV/opt	0.78	0.008
IR/opt	0.75	0.03

(Piro, Matt & Ricci 1997; Fabian et al. 1986) and is observed in both radio-loud (e.g. 3C 273) and radio-quiet (e.g. E1821+643) sources (Warwick, Barstow & Yaqoob 1989; Turner 1990). Almost half of the 48 Seyfert-type AGN surveyed by Turner & Pounds (1989) showed evidence for a soft excess. This excess at soft X-ray energies is thought to be associated with emission from inner regions of an accretion disc (Saxton et al. 1993). Although III Zw 2 is extremely luminous $L_{X(2-10)} = 10^{44}$–10^{45} erg s^{-1}, study of spectra over a 25-yr period does not reveal an excess at soft X-ray energies. One possible explanation for this absence could be that the soft excess in III Zw 2 contributes significantly only at energies below 0.2 keV. This suggests a lower disc temperature with a peak possibly in the UV region, but this is also not observed. Another possible explanation is that the soft excess is relatively weak compared with the power-law continuum emission; for example, as could be the case if the power-law continuum has contributions from other sources (e.g. synchrotron or synchrotron self-Compton emission from the jets) in addition to the Comptonized and reflected component.

We do not find significant evidence of absorption intrinsic to the source in the *XMM* or archival data studied here. This is in agreement with the findings of previous observations (Hall et al. 1981; Petre et al. 1984; Kaastra & de Korte 1988) and inferences from the IR/optical observations (Ward et al. 1987; Carleton et al. 1987). We do, however, detect a strong reflection component ($R = 2$) in the *XMM* data, a period when the X-ray flux of III Zw 2 was very low (Figs 6 and 7). The RGS spectrum is almost featureless except for a weak emission feature consistent with the forbidden [O VII] emission line. Such an emission line is expected from a photoionized plasma at relatively low ($<10^5$ K) temperature and density ($<10^{10}$ cm^{-3}) (Porquet & Dubau 2000). There is no evidence of edge-like or sawtooth spectral features that are seen in some Seyferts and are associated with relativistic disc lines or absorption edges from a warm absorber in our line of sight (Branduardi-Raymont et al. 2001; Lee et al. 2001).

The line emission between 6 and 7 keV in AGN is thought to be Fe Kα from neutral or ionized material. The line could arise owing to the X-ray irradiation of dense, relatively cold ($T \leqslant 10^6$ K) gas, in either an accretion disc around the central black hole (George & Fabian 1991; Matt, Perola & Piro 1991) or in more distant, neutral material, such as a molecular torus (e.g. Mrk 205, Reeves et al. 2001). A study of *ASCA* Seyfert I iron lines (Nandra et al. 1997) shows that Fe profiles show a broadening primarily to the red, a core energy close to 6.4 keV and relatively little flux blueward of 6.4 keV. The 6.44-keV line in the *XMM* spectra has a velocity width of FWHM $\sim$ 140 000 km s^{-1}, implying relativistic velocities. The large velocity width rules out emission from a torus. If we assume that the observed linewidth is caused by Doppler broadening in a relativistic accretion disc, it would require the line emission to originate very close to the black hole, where relativistic velocities are expected (Nandra et al. 1997).

However, the accretion disc model fit (for inclination $\leqslant 40^\circ$) to the observed line emission yields a line at 7.63 keV (disc–line) and 8.60 keV (Laor) which is inconsistent with Fe Kα emission (6.4–6.97 keV). The equivalent width of the line measured from the incident+reflected spectra is large (EW $\sim$ 800 eV). Theoretical work on iron lines predicts the intrinsic Fe line EW to be 100–200 eV, depending on the viewing angle (Fabian et al. 1989). Disc models incorporating relativistic effects have been able to increase iron-line EW to about 300 eV for low disc inclinations (Dabrowski et al. 2001). Recent work by Ballantyne et al. (2002) shows that the largest EWs measured from the incident+reflected spectra are $\sim$800 eV when the gas is ionized. If this model is correct it could explain the observed EW in III Zw 2 but not the high line energy,

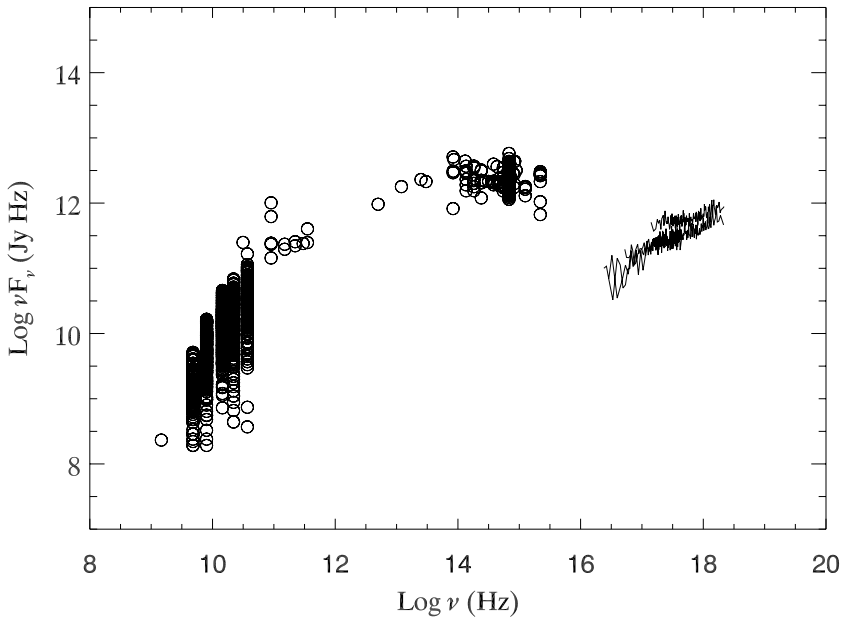

Figure 8. Spectral energy distribution for III Zw 2. It includes radio to X-ray data taken over the last three decades.

which would require significant blueshifting of the Fe Kα emission in the disc. This suggests that the existing disc models are unable to adequately describe the excess emission between 5.5 and 7.5 keV in III Zw 2.

In general, unlike III Zw 2, luminous radio-loud quasars tend to have weaker Fe line emission (Reeves & Turner 2000). However, it should be noted that although III Zw 2 is very luminous and exhibits large radio flares, it is not a typical radio-loud quasar, but it is instead classed as a radio-intermediate quasar, i.e. a radio-weak quasar but with relativistic jets pointed straight at the observer (Falcke et al. 1999). One possibility for the observed line profile is contributions of iron-line emission from the base of the subparsec jet system of III Zw 2, perhaps in addition to the disc emission. Of the 24 type I AGN studied by Reynolds (1997), velocity widths corresponding to FWHM $> 100\,000$ km s^{-1} and EW ~ 1.0 keV have been observed in only two X-ray-luminous ($L_{2-10} > 10^{44}$ erg s^{-1}) galaxies, 3C 120 and 3C 382, both radio-loud sources exhibiting superluminal motion. Contribution of unresolved, Doppler-shifted Fe emission from the base of relativistic jets and/or ejecta in addition to disc emission could be one possible explanation for the large velocity width, EW and the high line energy of the observed emission between 5.5–7.5 keV. Doppler-shifted iron-line emission from the approaching and the receding relativistic jets has been observed in the Galactic source SS 433 (Marshal et al. 2002).

4.2 X-ray variability

Long-term X-ray variability is known to be a common phenomenon in AGN (Grandi et al. 1992) but rapid variability is typically not detected in high-luminosity AGN (Green et al. 1993). III Zw 2 exhibits large-amplitude (10-fold) X-ray variability over time-scales of years but we do not detect significant variations in X-ray flux over short time-scales (few 1000 s) in any of the data.

In order for variations in flux to be observed, the variability time-scales must be larger than the source light crossing time. As such, rapid variations allow us to place upper limits on the mass of the central black hole. Based on reports of a 1000–1500 s flare in III Zw 2 (Pounds 1986), Kaastra & de Korte (1988) have estimated a black hole mass of $\sim 10^7$ M$_\odot$ for the source. We do not detect any swift changes in X-ray flux [that supports the findings of Tagliaferri et al. (1988) where it was suggested that the flare detected in III Zw 2 may be associated with the nearby star HD 560] and hence do not require such a low-mass black hole to explain the X-ray variability in III Zw 2.

Luminous sources such as III Zw 2 are expected to have larger X-ray-emitting regions than lower-luminosity Seyferts, possibly because they have more massive central black holes (Green et al. 1993; Saxton et al. 1993). We consider that the high X-ray luminosity and the lack of short-term variability hints at the presence of a large-mass black hole ($\geqslant 10^9$ M$_\odot$) at the centre of III Zw 2. The absence of a blackbody component at low X-ray energies is consistent with this picture, as the disc around such a massive black hole would be formed further away and hence would have a lower temperature. Using the mass relationship from Wandel (1999) and the observed Hβ FWHM of III Zw 2 (5200 km s^{-1}, Wilkes 1986) we infer a black hole mass of $\sim 10^9$ M$_\odot$, which is consistent with the lack of rapid variability in the source and is comparable with the mass estimate obtained from O III linewidths by Wandel & Mushotzky (1986).

4.3 Multiwavelength emission

AGN emit radiation across a wide frequency range, from X-rays to radio. The X-rays are thought to arise from regions very close to the central black hole. Leading models based on the observed power-law X-ray spectra in AGN explain the X-ray emission in terms of a hot Comptonizing corona that up-scatters softer disc photons to produce the hard X-ray continuum. The optical and UV radiation is considered to be thermal emission from an accretion disc, with the optical radiation arising from outer parts of the disc. The infrared is generally emission from hot dust, but in some cases has a non-thermal origin. The radio emission is synchrotron radiation from relativistic jets. Since the emission in the different wavebands arises from separate emission mechanisms we would not generally expect them to be closely related.

Rapid X-ray variability is generally found to be unrelated to the optical variations in AGN. However, on time-scales of several weeks or more, correlated X-ray and the optical temporal variations have been recently detected in NGC 7469 (Nandra et al. 2000) and NGC 4051 (Peterson, McHardy & Wilkes 2000). Related X-ray and *K*-band emission has been observed in the radio-loud AGN 3C 273 (McHardy et al. 1999). Although correlated radio and optical emission on long time-scales has been reported in a few AGN (Clements et al. 1995), broad-band coordinated activity from the X-rays to the radio is rare. The multiwavelength emission of III Zw 2 shows coordinated behaviour from X-ray to radio wavelengths. The absence of a big blue bump in the broad-band spectrum contrasts with typical AGN in which a substantial proportion of UV/X-rays are thought to be emitted from an optically thick accretion disc (cf. Kaastra & de Korte 1988). The large-amplitude flare observed in all wavelengths around 1980 suggests that the emission from the X-ray to radio wavelengths could have a common origin. The radio emission in radio-loud AGN is thought to be synchrotron radiation. Optical microvariability was recently detected in III Zw 2 where the source flux increased by 0.1 mag in about 4 h (Jang & Miller 1997), which suggests a compact emission region. Jang & Miller (1997) have found that most AGN that exhibit microvariability are radio-loud and have argued that microvariability is associated with the jets in these sources. If this model is correct it would imply that at least some of the optical emission in III Zw 2 is of non-thermal origin.

The spectral energy distribution of III Zw 2 from the radio to the optical/UV wavelengths mimics a typical synchrotron spectrum: self-absorbed at low energies (radio/millimetre), power law over a broad wavelength range and a cut-off at high energies. It is unlikely that the turnover in optical/UV wavelengths is caused by absorption as we do not find evidence of intrinsic absorption in the X-ray band and the source exhibits minimum reddening compared with the other hard X-ray-selected objects of the Piccinoti et al. (1982) sample (Carleton et al. 1987). One can explain the observed SED, optical microvariability and the related behaviour at different wavelengths if the broad-band emission from 10^9–10^{14} Hz is due to synchrotron radiation from an expanding magnetized cloud of relativistic electrons. If this is the case the synchrotron emission would be self-absorbed in the radio-millimetre region and would have a high-energy cut-off at frequencies greater than 10^{14} Hz.

The X-ray radiation is not consistent with a synchrotron spectrum that would produce the radio and optical emission and hence has to be a separate component. However, the X-ray emission is found to be significantly correlated with the optical band, which implies a close link between the two wavebands. The X-ray radiation has a power-law shape typical of Compton up-scattered emission. If a hot Comptonizing corona close to the disc were responsible for all the X-ray radiation it would be difficult to explain the correlation with the synchrotron optical emission.

A simple explanation for the observed coincidence of X-ray flares with those at the other wavelengths would be that some of the X-ray

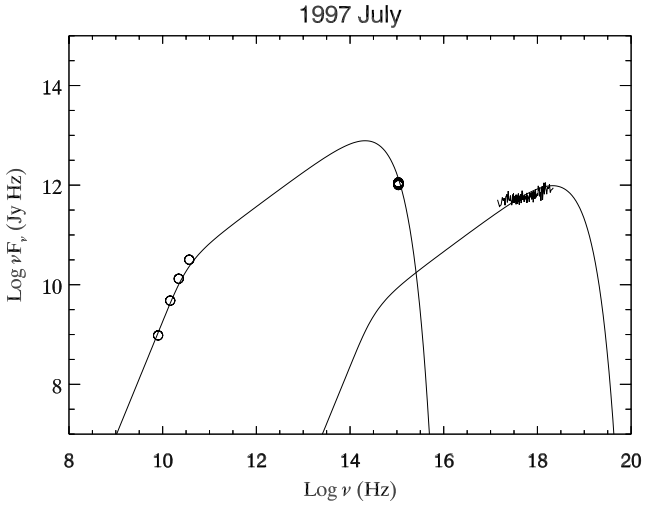

Figure 9. Radio to optical spectrum modelled as synchrotron radiation with peak frequency of 37 GHz, a high energy cut-off at 3×10^{14} Hz, $\alpha_{\rm thin} = 0.7$ and $\alpha_{\rm thick} = 1.3$. The X-rays are modelled as Compton up-scattered synchrotron radiation for a source size of 0.07 mas and $\delta = 1$.

emission is a result of Compton up-scattering by the high-energy relativistic electrons that give rise to synchrotron radio and optical/IR radiation. Electron Lorentz factors of $\gamma_{\rm e} \sim 400$ have been measured in the radio band in III Zw 2 (Falcke et al. 1999), which are sufficient to up-scatter IR/optical photons to X-ray energies. The strong reflection that we measure requires that a substantial fraction of the X-rays produced by this process must also be reflected in addition to the X-rays produced by Compton up-scattering in the corona. Since the jets in III Zw 2 are quite small (subparsec scale), X-rays emitted by the jets may indeed see a large solid angle of the reflector.

We have modelled the observed radio to optical spectrum (of 1997 July) as synchrotron radiation and X-rays as Compton up-scattered synchrotron radiation (Bloom & Marscher 1996). We use a source size of 0.07 mas and $\alpha_{\rm thin} = 0.7$ measured at 43 GHz during the 1997–1999 flare (Falcke et al. 1999; Brunthaler et al. 2000). We assume no relativistic beaming, i.e. $\delta = 1$. Fig. 9 shows a model fit to the 1997 July spectrum. The observed radio to optical emission is well described by a synchrotron spectrum with peak frequency of 37 GHz and a high-energy cut-off at 3×10^{14} Hz. The best-fitting spectral index for the optically thick region of the synchrotron spectrum is $\alpha_{\rm thick} = 1.3$, which is indicative of an inhomogeneous source (Bloom et al. 1999).

5 CONCLUSION

We have studied the X-ray emission in III Zw 2 over three decades and find that the basic shape of the X-ray spectrum is a power law with photon index $\Gamma \approx 1.7$. We do not find an excess at soft X-ray energies and the absorption is consistent with the line-of-sight Galactic column density. The *XMM* and *ASCA* spectra show excess emission between 5.5 and 7.5 keV, which cannot be entirely explained in terms of fluorescence Fe Kα emission from a low-inclination relativistic disc. A contribution from the relativistic jets and/or ejecta to the Fe Kα emission could explain the observed line profile in III Zw 2.

We observe large-amplitude (10-fold) flux variations in the 25 yr X-ray light curve, however, we do not detect significant rapid variations (few 10^3 s) in flux, in the individual observations, which is consistent with a large-mass black hole in this system. We infer a black hole mass of $\sim 10^9$ $M_\odot$ (from Hβ FWHM) for III Zw 2, which is much higher than some previous estimates.

Multiwavelength light curves show related variations from the radio to X-ray wavelengths. We interpret the radio to optical emission as synchrotron radiation, self-absorbed in the radio/millimetre region, and the X-rays as mainly a result of Compton up-scattering of low-energy photons by the population of high-energy electrons that give rise to the synchrotron radiation.

ACKNOWLEDGMENTS

We would like to thank J. Mittaz for his support and guidance in the reduction of the archival data. The operation of the UMRAO 26-m telescope is supported by the University of Michigan Department of Astronomy. ERC would like to thank D. Lancy for his assistance with the acquisition and analysis of the SAAO IR data and D. Romero, E. Colmenero and S. Potter for their continued support. NJS acknowledges the receipt of a PPARC studentship.

REFERENCES

Aller H. D., Aller M. F., Latimer G. E., Hodge P. E., 1985, ApJS, 59, 513
Andrews D., 1984, EXOSAT Express, 3, 1
Ballantyne D. R., Fabian A. C., Ross R. R., 2002, MNRAS, 329, L67
Bleeker J. A. M., 1975, ESA X-Ray Astronomy and Related Topics, Vol. 89
Bloom S. D., Marscher A. P., 1996, ApJ, 461, 657
BloomS. D., Marscher A. P., Moore E. M., Gear W., Teräsranta H., Valtaoja E., Aller H. D., Aller M. F., 1999, ApJS, 122, 1
Briel U. G., Pfeffermann E., Hartner G., Hasinger, G., 1988, X-ray Instrumentation in Astronomony II, p. 401
Bon E., Popovic C., Mediavilla L. E. G., 2001, Astronomische Gesellschaft Abstract Ser. Vol. 18, 175
Branduardi-Raymont G., Sako M., Kahn S. M., Brinkman A. C., Kaastra J. S., Page M. J., 2001, A&A, 2001, 365, L140
Brunthaler A. et al., 2000, A&A, 357, L45
Carleton N. P., Elvis M., Fabbiano G., Willner S. P., Lawrence A., Ward M., 1987, ApJ, 318, 595
Carter B. S., 1990, MNRAS, 242, 1
Chapman G. N. F., Geller M. J., Huchra, J. P., 1985, ApJ, 297, 151
Clements S. D., Smith A. G., Aller H. D., Aller M. F., 1995, AJ, 110, 529
Condon J. J., O'Dell S. L., Puschell J. J., Stein W. A., 1981, ApJ, 246, 624
Dabrowski Y., Lasenby A. N., 2001, MNRAS, 321, 605
Dabrowski Y., Fabian A. C., Iwasawa K., Lasenby A. N., Reynolds C. S., 1997, MNRAS, 288, L11
de Robertis M., 1985, ApJ, 289, 67
den Herder J. W. et al., 2001, A&A, L7
Edelson R. A., Malkan M. A., 1987, ApJ, 323, 516
Elvis M. et al., 1994, ApJS, 95, 1
Fabian A. C., Guilbert P. W., Arnaud K. A., Shafer R. A., Tennant A. F., Ward M. J., 1986, MNRAS, 218, 457
Fabian A. C., Rees M. J., Stella L., White N. E., 1989, MNRAS, 238, 729
Falcke H. et al., 1999, ApJ, 514, L17
George I. M., Fabian A. C., 1991, MNRAS, 249, 352
Grandi P., Tagliaferri G., Giommi P., Barr P., Palumbo G. G. C., 1992, ApJS, 82, 93
Giacconi R. et al., 1979, ApJ, 230, 540
Green A. R., McHardy I. M., Lehto H. J., 1993, MNRAS, 265, 664
Hall R., Rickett M. J., Page C. G., Pounds K. A., 1981, Sp. Sci. Rev., 30, 47
Haardt F., Maraschi L., Ghisellini G., 1994, ApJ, 432, L95
Harris D. E., Stern C. P., Biretta J. A., 1990, Imaging X-Ray Astronomy. Cambridge University Press, Cambridge, p. 299
Holland W. S. et al., 1999, MNRAS, 303, 659
Hyland A. R., Allen D. A., 1982, MNRAS 199, 943
Inoue H., 1993, Exp. Astron., 4, 1
Jang M., Miller H. R., 1997, AJ, 114, 565

Jansen F. et al., 2001, A&A, 365, L1
Kaastra J. S., de Korte P. A. J., 1988, A&A, 198, 16
Kotilainen J. K., Ward M. J., Boisson C., Depoy D. L., Smith M. G., Bryant L. R., 1992, MNRAS, 256, 125
Kotilainen J. K., Ward M. J., Williger G. M., 1993, MNRAS 263, 655
Kukula M. J., Dunlop J. S., Hughes D. H., Rawlings S., 1998, MNRAS, 297, 366
Landau R., Epstein, E. E., Rather, J. D. G., 1980, AJ, 85, 363
Laor A., 1991, ApJ, 376, 90
Lebofsky M. J., Rieke, G. H., 1980, Nat, 284, 410
Lee et al., 2001, ApJ, 554, L13
Lloyd C., 1984, MNRAS, 209, 697
McAlary C. W., McLaren R. A., McGonegal R. J., Maza, J., 1983, ApJS, 52, 341
McHardy, Lawson A., Newsam A., Marscher A., Robson I., Stevens J., 1999, MNRAS, 310, 571
Marshall H. L., Canizares C. R., Schulz N. S., 2002, ApJ, 564, 941
Masnou J. L., Wilkes B. J., Elvis M., McDowell J. C., Arnaud K. A., 1992, A&A, 253, 35
Matt G., Perola G. C., Piro L., 1991, A&A, 247, 25
Nandra K., George I. M., Mushotzky R. F., Turner T. J., Yaqoob T., 1997, ApJ, 477, 602
Nandra K., Le T., George I. M., Edelson R. A., Mushotzky R. F., Peterson B. M., Turner T. J., 2000, ApJ, 544, 734
Neugebauer G., Oke J. B., Becklin E. E., Matthews K., 1979, ApJ, 230, 79
Peterson B. M., McHardy I. M., Wilkes B. J., 2000, New Astron. Rev., 44, 491
Petre R., Mushotzsky R. F., Krolik J. H., Holt S. S., 1984, ApJ, 280, 499
Pfeffermann E. et al., 1987, Presented at the Society for Photo-Optical Instrumentation Engineers. SPIE, Berlin
Piccinotti G., Mushotzky R. F., Boldt E. A., Holt S. S., Marshall F., Serlemitsos P. J., Shafer R. A., 1982, ApJ, 253, 485
Piro L., Matt G., Ricci R., 1997, A&AS, 126, 525
Porquet D., Dubau J., 2000, A&A, 143, 495
Pounds K. A., 1986, in Treves A., ed., Variability of Galactic and Extragalactic X-ray Sources. Associazone Per l'Avanzamento Dell'Astronomia, p. 1
Reeves J. N., Turner M. J. L., 2000, MNRAS, 316, 234
Reeves J. N. et al., 2001, A&A, 365, L134
Reynolds C. S., 1997, MNRAS, 286, 513
Rieke G. H., Lebofsky M. J., 1979, ApJ, 227, 710
Saxton R. D., Turner M. J. L., Williams O. R., Stewart G. C., Ohashi T., Kii T., 1993, MNRAS, 262, 63
Schnopper H. W. et al., 1978, ApJ, 222, L91
Sembay S., Hanson C. G., Coe M. J., 1987, MNRAS, 226, 137
Strüder L. et al., 2001, A&A, L18
Tagliaferri G., Giommi P., Angelini L., Osborne J. P., Pallavicini R., 1988, ApJ, 331, L113
Teräsranta H. et al., 1998, A&AS, 132, 305
Turner M. J. L., 1990, MNRAS, 244, 310
Turner M. J. L., Smith A., Zimmermann H. U., 1981, Space Sci. Rev., 30, 513
Turner M. J. L. et al., 2000, A&A, L27
Turner T. J., Pounds K. A., 1989, MNRAS, 240, 833
Voges W. et al., 1999, A&A, 349, 389
Wandel A., 1999, ApJ, 527, 649
Wandel A., Mushotzky R. F., 1986, ApJ, 306, L61
Ward M., Elvis M., Fabbiano G., Carleton N. P., Willner S. P., Lawrence A., 1987, ApJ, 315, 74
Warwick R. S., Barstow M. A., Yaqoob T., 1989, MNRAS, 238, 917
Wilkes B. J., 1986, MNRAS, 218, 331
Wilkes B. J., Masnou J.-L., Elvis M., McDowell J., Arnaud K., 1989, in 23rd ESLAB Symposium on Two Topics in X Ray Astronomy, Vol. 2. ESA, Noordwijk, p. 1081
Wright A. E., Allen D. A., Krug P. A., Morton D. C., Smith M. G., 1977, IAU Circ. 31452

This paper has been typeset from a TEX/LATEX file prepared by the author.